Correlation between dynamical heterogeneities, structure and potential-energy distribution in a 2D amorphous solid. — Source link

Sylvain Mazoyer, Florian Ebert, Georg Maret, Peter Keim

Institutions: University of Konstanz

Related papers:

- Direct observation of a local structural mechanism for dynamic arrest.

- Theoretical perspective on the glass transition and amorphous materials

- Roles of icosahedral and crystal-like order in the hard spheres glass transition

- Understanding fragility in supercooled Lennard-Jones mixtures. I. Locally preferred structures

- Growing static and dynamic length scales in a glass-forming liquid.

Correlation between dynamical heterogeneities, structure and potential-energy distribution in a 2D amorphous solid

S. Mazoyer, F. Ebert, G. Maret, and P. Keim[a]

Fachbereich Physik, Universität Konstanz, D-78457 Konstanz, Germany

Abstract. We investigate the collective properties of particles in a 2D experimental system which consists of a bi-disperse mixture of colloidal particles confined at an air/water interface. We find a direct correlation between structure and dynamical heterogeneities in this system: particles belonging to locally ordered structures have lower potential energy and are slower than other particles. In a more general way we show that particles with high potential energy are dominating the dynamics especially in the α-relaxation regime.

1 Introduction

The microscopic processes responsible for solidification of supercooled fluids near the glass transition are still poorly understood. Dynamic heterogeneities are believed to be a key feature in the understanding of the relaxation behavior near structural arrest. They are commonly evoked to explain intriguing properties of the dynamics like non-exponential relaxation functions and two-time relaxation [1–6]. Great progress in their study has been made thanks to direct real space observation of colloidal systems and the existence of populations of fast and slow particles forming clusters of a few tens of fast particles has been shown for instance in [7,8]. Dynamical heterogeneities are also evoked to explain diverging length scales upon cooling as their characteristic length scale is believed to grow when approaching the glass transition [1,3,9,10]. Many attempts have been made to find a link between dynamical heterogeneities and structures [11–17].

Based on numerical simulations of hard disks, Tanaka *et al.* [18,19] have observed a correlation between medium-range crystalline order (MRCO) and clusters of slowest particles in the α-relaxation regime. Using MD simulations, Matharoo *et al.* [20] have shown low mobility of clusters of low-potential-energy molecules for water in the supercooled phase. Yet another approach is to analyze the predictability of the long time dynamics of the particles from their short-time behavior. Widmer-Cooper and Harrowell introduced the iso-configurational ensemble, a set of initial situations with the same positions but different momenta of the particles and have tried to show a connection between dynamical properties of a particle with its local environment [21,22].

While most of these studies of dynamical heterogeneities have been performed by simulations, experimental work in direct space remains still rare [7,8,23]. In this letter we present results from an experimental study of a 2D colloidal system which consists of a binary mixture of super-paramagnetic particles interacting via a dipole-dipole potential. The strength of the interaction is fixed by an external magnetic field, so direct observation of the particle positions provides knowledge of the potential energy for each particle. We show that locally symmetric structures have slower dynamics and regions of slow dynamics which are visible as dynamical heterogeneities have lower potential energy at the same time.

2 Experimental setup

Our experimental setup has been described elsewhere [24]. The system consists of a suspension of two kinds of spherical super-paramagnetic colloidal particles A and B with different diameters ($d_A = 4.5\,\mu$m, $d_B = 2.8\,\mu$m) and magnetic susceptibilities ($\chi_A \approx 10 \cdot \chi_B$). Due to their high mass density of $\rho_m \approx 1.5\,$g/cm^3, particles are confined by gravity to the water-air interface formed by a pending water drop suspended by surface tension in a top sealed cylindrical hole (6 mm diameter, 1 mm depth) in a glass plate, see fig. 1. A magnetic field $\mathbf{H}$ applied normal to the water-air interface induces a magnetic moment $\mathbf{M} = \chi\mathbf{H}$ in each particle leading to a repulsive dipole-dipole pair interaction.

The control parameter Γ which quantifies the strength of the interaction is defined by the ratio between average magnetic interaction energy and thermal energy

$$\Gamma = \frac{\mu_0}{4\pi} \frac{H^2 \cdot (\pi\rho)^{(3/2)}}{k_B T} (\xi \cdot \chi_B + (1-\xi) \cdot \chi_A)^2, \quad (1)$$

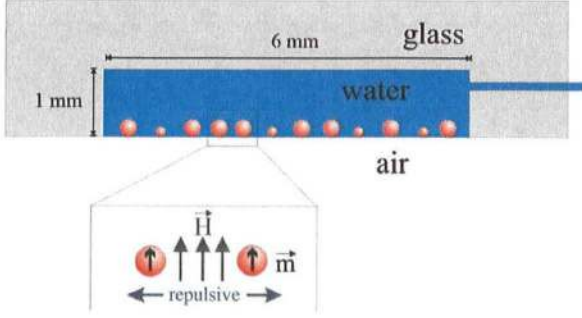[a] e-mail: `peter.keim@uni-konstanz.de`

Fig. 1. Super-paramagnetic colloidal particles (not to scale) confined at a water-air interface due to gravity. A tunable magnetic field induces a repulsive dipole interaction between the particles.

where ρ is the 2D area density of the particles, ξ denotes the relative fraction of small particles $\xi = N_B/(N_A + N_B)$, where N_A, N_B are the numbers of big and small particles in the field of view. Particles are visualized by video microscopy using an 8-bit CCD camera. The field of view has a size of $\approx 1\,\mathrm{mm}^2$ containing typically 3×10^3 particles, while the whole sample contains up to 10^5 particles. Standard image processing provides size, number, and positions of the colloids with a resolution better than $50\,\mathrm{nm}$. A computer-controlled syringe driven by a micro stage controls the volume of the droplet to reach a completely flat surface.

To achieve a horizontal interface, the inclination of the whole experimental setup is controlled actively by microstages with a resolution of $\Delta\alpha \approx 1\,\mu\mathrm{rad}$. Trajectories of all particles in the field of view can be recorded over several days providing information on all relevant time and length scales. Furthermore, the pair interaction can also be directly controlled over a wide range. In this geometry the dipolar pair potential of particle i is given by

$$E_p^i(r) = \frac{\mu_0}{8\pi} \sum_{j=1}^{N} \frac{\chi_i \cdot \chi_j \cdot H^2}{r_{ij}^3}, \qquad (2)$$

where j runs over all other particles, r_{ij} is the distance between particle i and j and χ_i the magnetic susceptibility of the particle i. In refs. [25–27] we described that our system has local crystalline but no long range order [28] and shows glassy dynamics. The crystallites found are mainly of two kinds. One has hexagonal symmetry and is made only of big particles which corresponds to the crystalline order observed in the solid phase for the mono-disperse system. The other has square symmetry and is composed of big particles at the corners and a small one in the center.

For the given mixing ratio the square crystallite might be seen as the 2D analogon of locally favored structures [15, 16] found in simulation and colloidal gels in 3D. Both types of 2D-crystallites are able to build up some compact grains made of several cells having identical orientation [25, 28]. Those crystalline grains are compatible with the crystal lattice being the ground state configuration for the given mixing and susceptibility ratio where

the ground state configurations were calculated by lattice sums [29] and genetic algorithms [30]. Even when the system is quenched abruptly from the fluid phase into the amorphous solid state ($\Gamma = 1$ to $\Gamma = 390$) small crystallites with square and hexagonal symmetry appear. It was suggested in simulations [27] that these locally ordered structures have lower dynamics than the disordered parts of the sample.

3 Dynamics of locally favored structures

In order to detect the hexagonal structures in the quasi-equilibrium sample studied here, we use a bond angle deviation parameter a which quantifies the deviation from an average angle between two adjacent bonds,

$$a = \sqrt{\frac{1}{N_{nn}} \sum_{j=1}^{N_{nn}} (\Theta_{\widehat{kij}} - \overline{\Theta})^2 \cdot \frac{1}{\overline{\Theta}}}, \qquad (3)$$

where $\Theta_{\widehat{kij}}$ is the angle between two successive bonds formed by particles i and k, and i and j, respectively. $\overline{\Theta}$ is the average of $\Theta_{\widehat{kij}}$ over all the bonds formed by particle i and the nearest neighbors. As in [25] a second criterion is necessary and we use the bond length deviation parameter b

$$b = \sqrt{\frac{1}{N_{nn}} \sum_{j=1}^{N_{nn}} (l_{ij} - \bar{l})^2 \cdot \frac{1}{\bar{l}}}, \qquad (4)$$

where l_{ij} is the length of the bond between particle i and particle j and $\bar{l}$ is the average of l_{ij} over all nearest neighbors. For a small particle to belong to a square structure we used the criteria $a < 0.1$, $b < 0.1$ and that its four nearest neighbors must be big particles. For the hexagonal structure the six nearest neighbors must be big particles. This combination of criteria is quite natural and has the advantage to select particles which are intuitively selected by eye and discards the others. In order to study the influence of the crystallite's symmetry on the dynamics we watch out for particles which satisfy both criteria for a and b during at least 10% of the total duration of the experiment. This condition is largely flexible enough for a particle to eventually fluctuate around its symmetric configuration.

Particles escaping from their cages are often believed to be responsible for the α-relaxation seen in the mean-square displacement (MSD). In [31] we have shown that this hopping-out-of-cage dynamics of individual particles was possibly hidden by some collective unidirectional motion of particles with their cage. Therefore we investigated the displacement of a colloid with respect to the average displacement of its nearest neighbors. This cage-relative position is defined as

$$r_{\mathrm{CR}}^i(t) = r^i(t) - (r_{nn}^i(t) - r_{nn}^i(0)), \qquad (5)$$

where i is the index of the particle, $r^i(t)$ its position at time t and $r_{nn}^i(t)$ is the position of the center of

mass of the initially (at $t = 0$) nearest neighbors: $\boldsymbol{r}_{nn}^{i} = \frac{1}{N_{nn}} \sum_{j=1}^{N_{nn}} (\boldsymbol{r}^{j}(t) - \boldsymbol{r}^{j}(0))$, where j runs over the indices of the nearest neighbors defined by Voronoi tessellation and N_{nn} is the number of nearest neighbors. This cage-relative position and associated cage-relative MSD have been successfully used in simulations [32] and experiments [33] of crystallizing systems to determine the melting temperature in 2D. In [31] we used it to discriminate between cage motion and particles motion relatively to their cage near the glass transition. Thanks to this, a cage dynamics has been visualized in the amorphous solid phase. Particles first explore the environment made up by the surrounding neighbors. Later, in the plateau regime of the MSD, a few particles start to make some hopping processes, a phenomenon which becomes more frequent in the α-regime. In addition, particles also move collectively with their cages, especially in the plateau and α-relaxation regimes.

In fig. 2 we have plotted the cage-relative mean-square displacement (CR-MSD) of both small (panel a) and big (panel b) particles selected according to their affiliation to a given crystalline cell type for $\Gamma = 338$. For this value of the control parameter Γ, we name the system an amorphous solid. To do so (and since we cannot measure T_G by the viscosity in a 2D system) we have analysed the low-frequency shear modulus μ of the colloidal ensemble and determined the transition temperature in units of Γ between amorphous solid and fluid by the extrapolation to a zero-frequency shear modulus. The system is fluid $\mu \simeq 0$ for $\Gamma \leq 169$ and solid $\mu > 0$ for $\Gamma \geq 242$ [34].

In the short-time regime and the beginning of the plateau the two curves superimpose while at the end of the plateau the CR-MSD of small particles belonging to a square structure is clearly smaller than the average curve. So, with respect to their cage, small particles in the middle of a square structure move less than the others. This is the same for big particles belonging to the shell of a hexagonal structure and even more pronounced for those being the center of a hexagon. Particles in a high symmetry configuration of the local environment, where we know that the global structure with similar global stoichiometry corresponds to the energetic ground state [29,30], are on average less mobile.

The difference in the amplitude of the CR-MSD between small a) and and big b) particles was suggested to be interpreted in terms of decoupling of the dynamics between both species. In [35,36] this decoupling is investigated for highly asymmetric systems like colloid-polymer mixtures or soft mixtures like star-star-polymers where depletion forces play a crucial role. However, in [37] we have shown that our binary mixture is negative non-additive and depletion forces do not play any role. According to [5] the investigation of the classical MSD shows that the different mobilities scale directly with the size ratio of the species which is $d_A/d_B = 1.6$ in the present experiment. Late in the the α-regime the ratio in dynamics increases slightly to a factor of about 2. This increase is slightly stronger visible (about 2.3) in the CR-MSD and can be interpreted as follows: small particles sometimes perform a jump out of the cage (see also fig. 3), whereas the big
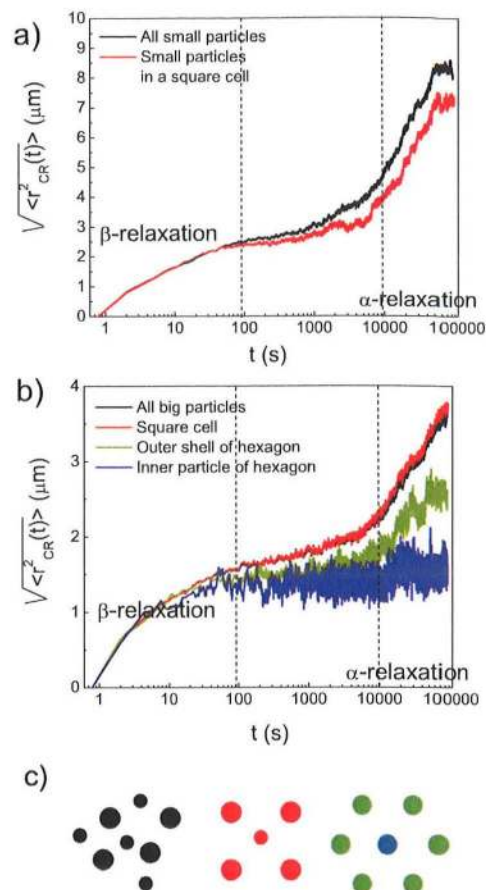

Fig. 2. (Color online) a) Lin-log plot of the root cage-relative mean-square displacement (CR-MSD) for small particles in different local configuration at $\Gamma = 338$. b) Same for the big particles. c) Color code for the local configurations; black corresponds to the average over all small particles a) and all big particles b). Red corresponds to local square order with a) a centered small particle and b) four big particles at the corner. Green corresponds to local hexagonal order (it appears only for the big particles) with blue being the center particle. The noise in blue curve is much larger, since only $\sim 1\%$ of the particles contribute to this mean value. Particles in the center of locally ordered structures have a smaller cage-relative mean-square displacement.

ones usually perform an intra-cage hopping process as rare event [31]. This again underlines the sensitivity of the CR-MSD to local mobilities but in our opinion should not be interpreted as decoupling in the dynamics between big and small particles, even if relaxation processes in the aging regime should turn out to be slightly different. To date, in the α-regime of the classical MSD, we cannot distinguish between diffusive or sub-diffusive behaviour and Mermin-Wagner fluctuations known from 2D crystals [38]. Note, that the amplitude of the CR-MSD is about $1.8\,\mu$m (big) and $3\,\mu$m (small) in the inflection point, much less than the typical inter-particle distance of $21\,\mu$m (big-big) or $16\,\mu$m (big-small).
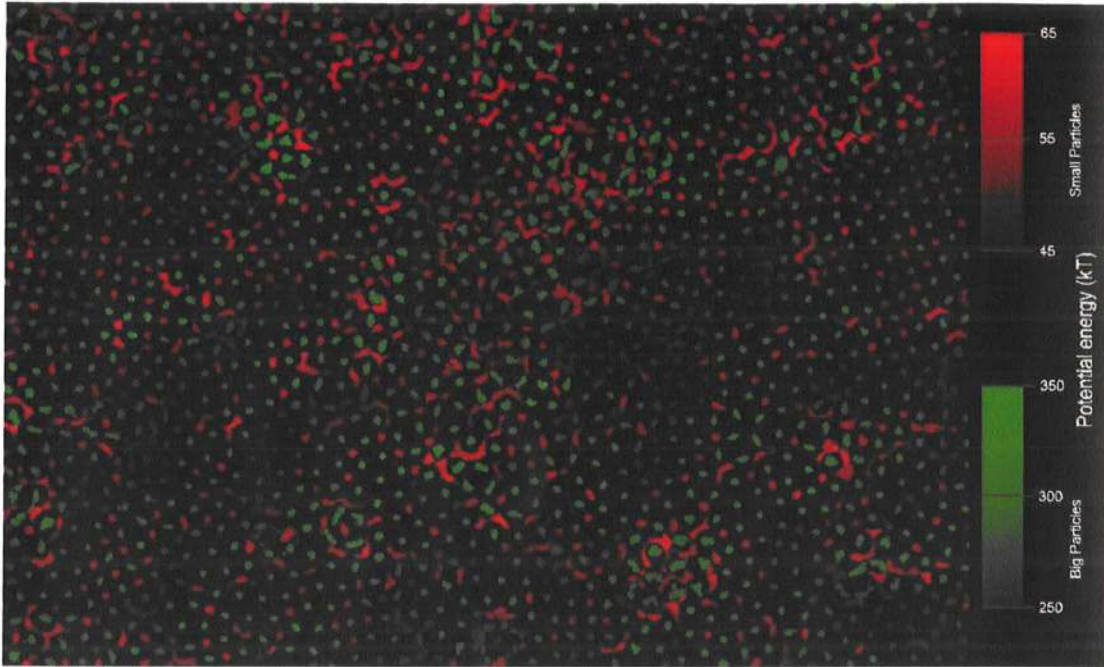
Fig. 3. (Color online) Cage-relative trajectories for big particles in green and small particles in red at $\Gamma = 338$. The intensity of the color is proportional to the potential energy of the particle averaged over the duration of the experiment ($t = 80000\,\mathrm{s}$).

4 Local dynamics versus potential energy

Now we focus on the mobility of all particles. Figure 3 shows the cage-relative trajectories of the big and small particles in green and red, respectively, for the total duration of the experiment ($t = 80000\,\mathrm{s}$). We observe that the dynamics with respect to the nearest neighbors is clearly heterogeneous and that in some large areas particles indeed perform some hopping processes. Plotting the trajectories for equivalent time windows shows that the heterogeneous patterns are static for measurements with $\Gamma \geq 242$. This is true for systems in the amorphous solid state which have been equilibrated for several days up to two weeks (not exactly the same waiting time for different measurements due to technical reasons) at a given effective temperature Γ. On the given time scale we do not observe temporal-spatial fluctuations of the patterns as has been reported in [7,8,39] for 3D systems or 2D systems [40] close to the glass transition. Here, we have to discuss the accessible time scales in our systems. The measurements cover five decades in time, a value which has to be compared with the short-time diffusion coefficient $D_0 = 0.11\,\mu\mathrm{m}^2/\mathrm{s}$ leading to a Brownian time (to diffuse the own diameter) of $\tau_B = 50\,\mathrm{s}$ for the big particles. Our accessible time scale is short compared to solid state experiments [41] but has to be related to the reduced stiffness of soft-matter systems *versus* solid-state systems which scales to be smaller by 15–18 orders of magnitude in 3D and still 10–12 orders of magnitude in 2D. It is this softness which "compresses" the physical processes in time.

The brightness of the trajectory plotted for individual particles in fig. 3 is proportional to the potential energy of the particle itself averaged over the duration of the experiment. To calculate the potential energy we have used eq. (2) but only neighbors closer than $120\,\mu\mathrm{m}$ are considered. This cutoff value corresponds to about six times the average inter-particle distances and the contribution of a particle outside this cutoff radius to the energy is less than 0.5%. It is important to note that the spatially heterogeneous distribution of the potential energies is static on the experimental time scale, too, which is in the α-relaxation regime. The system is not able to relax regions of high and low potential energy to a mean value within the given experimental time scale (including the waiting time), even if the full width half-maximum of the energy histogram (black curve in fig. 4) is about $\pm 10\%$ of the mean value for the small and $\pm 5\%$ for the big particles [1]. Therefore the spatial patterns of the energy distribution are very similar in the beginning and the end of the experiment. This is the reason why we averaged the potential energy of the particles for the duration of the experiment since we did not want to select a special time window. The presence of both dynamical and structural (in terms of potential energy) heterogeneities is obvious. More interestingly it is also evident that there is a significant correlation between them.

In order to quantify this connection between dynamical heterogeneities and structural quantities, we have plotted in fig. 4 a histogram of the number of particles per

---

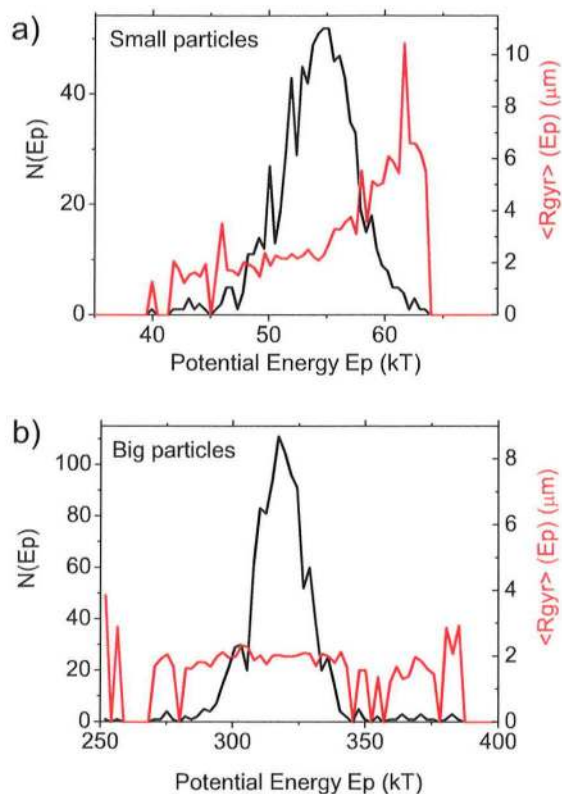[1] In a mono-disperse crystallizing sample this variation is less than 1%.

Fig. 4. (Color online) Number of particles $N_{(E_p)}$ per unit energy averaged over the total duration of experiment in black. Average cage-relative radius of gyration $\langle R_{\mathrm{gyr}}(E_p) \rangle$ per unit energy is in red. Small particles with high potential energy have a larger cage-relative radius of gyration of their trajectories.

potential energy (black curve) and the radius of gyration of the cage-relative trajectory as function of potential energy (red curve). The radius of gyration of the trajectories is defined as follows [42]:

$$R_{\mathrm{gyr}}^{i} = \sqrt{\frac{1}{N_t} \sum_{t=0}^{t_{\mathrm{exp}}} (\boldsymbol{r}^{i}(t) - \boldsymbol{r}_{\mathrm{CM}}^{i})^2}, \qquad (6)$$

where t runs over all experimental points, N_t is the number of experimental points, and t_{exp} the duration of the experiment. $\boldsymbol{r}_{\mathrm{CM}}^{i}$ is the center of mass of the cage-relative trajectory $\boldsymbol{r}_{\mathrm{CM}}^{i} = \frac{1}{N_t} \sum_{t=0}^{t_{\mathrm{exp}}} \boldsymbol{r}^{i}(t)$. We average the cage-relative radius of gyration $\langle R_{\mathrm{gyr}}(E_p) \rangle$ for all particles having their potential energy between E_p and $E_p + \Delta E_p$. We have also plotted the number of particles per unit of potential energy to indicate an estimation of the accuracy of the statistics. We see that for small particles $\langle R_{\mathrm{gyr}}(E_p) \rangle$ clearly increases with potential energy. Nevertheless, this correlation is not obvious for the big particles and the distribution of $\langle R_{\mathrm{gyr}}(E_p) \rangle$ is rather flat. We interpret this as follows: Small particles are sitting in deep potential minima and the thermal fluctuations within the cage are small, such that the motion of the potential minimum due
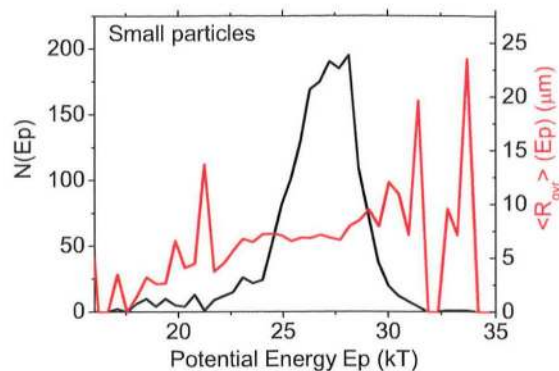

Fig. 5. (Color online) Same quantities as in fig. 4 for $\Gamma = 169$ in the supercooled state calculated for $1000\,\mathrm{s}$. This time corresponds to the inflection point of the mean-square displacement. For longer times this correlation is less visible.

to structural relaxations is clearly visible in their cage-relative mean-square displacement. Structural relaxations are supposed to be driven by decreasing the level of the potential minima towards the equilibrium configurations. The large radius of gyration of the small species is dominated by the reorganization of the local environment forcing the small particle to follow the motion of the local energetic minimum. On the other hand, the average potential minimum of large particles is about 5.5 times larger compared to the small ones (see color code of fig. 3 or maximum of the energy histogram in fig. 4). Therefore the curvature of the potential minimum has to be smaller. Big particles are allowed to explore the space around the local equilibrium position within the cage to a high extend, the Debye-Waller factor is large compared to the motion of the potential minima. This individual motion superimposes the effect seen for the small particles.

If we analyze data at lower interaction strength (higher effective temperatures) in the fluid state (where the zero-frequency shear modulus vanishes [34]) the dynamic behavior is qualitative different. In the fluid phase, for $\Gamma = 51$ the sample shows homogeneous dynamics. For $\Gamma = 110$ dynamical heterogeneities are visible only on short time scales and correlations between structure and dynamics are detectable only in the β-relaxation regime and diminish for longer times. Approaching the transition a correlation between structure and dynamics can be identified for longer time scales. Figure 5 shows the potential-energy distribution and radius of gyration analysed at $\Gamma = 169$ for $1000\,\mathrm{s}$ for small particles. This time window corresponds to the inflection point in the mean-square displacement. For longer time windows up to $20000\,\mathrm{s}$ this correlation diminishes indicating diffusive dynamics on long time scales and/or spatial-temporal fluctuations in the pattern of the dynamical heterogeneities. Since the average inter-particle distance is $16\,\mu\mathrm{m}$, one can identify a few colloids with high potential energy to escape out of their cage on this relatively short time scale.

5 Conclusions

In conclusion, we have shown evidence for a correlation between dynamical and structural heterogeneities in the supercooled fluid and amorphous solid state (in terms of zero-frequency shear modulus) and showed that regions of fast and slow moving particles are static for the time scale investigated in this experiment. Particles belonging to a structure with local symmetry such as squares for the small or hexagons for the big particles, respectively, have on average a slower dynamics with respect to their cage. The locally ordered structures correspond to the ground state configurations of the system for the given mixing and susceptibility ratio. The mobility of small particles is correlated to the potential energy —particles with high potential energy are more mobile than those with low energy. This is true for all analysed data in the amorphous solid state at $\Gamma = 242, 338, 390$. In the fluid phase for $\Gamma = 51, 110$ the dynamics is (almost) homogeneous. Approaching the transition at $\Gamma = 169$ a correlation of potential energy and fast moving particles can be found in a time window of $1000\,$s. For longer times this correlation diminishes due to the diffusive behavior of the sample.

Attention must be paid to the fact that the link we have found implies the dynamics of particles with respect to their cage. In [31] we have seen that the usual behavior of cage dynamics observed in 3D systems is the same as that one observed in this 2D system when we investigate the behavior of particles with respect to their initially nearest neighbors. This may be due to long-wavelength density fluctuations which are known in 2D crystals [38] but yet to be found in 2D amorphous solids.

References

1. W. Kob, C. Donati, S.J. Plimpton, P.H. Poole, S.C. Glotzer, Phys. Rev. Lett. **79**, 2827 (1997).
2. C. Donati, J.F. Douglas, W. Kob, S.J. Plimpton, P.H. Poole, S.C. Glotzer, Phys. Rev. Lett. **80**, 2338 (1998).
3. L. Berthier, G. Biroli, J.P. Bouchaud, L. Cipelletti, D. El Masri, D. L'Hôte, F. Ladieu, M. Pierno, Science **310**, 1797 (2005).
4. L. Berthier, D. Chandler, J.P. Garrahan, Europhys. Lett. **69**, 320 (2005).
5. H. König, R. Hund, K. Zahn, G. Maret, Eur. Phys. J. E **18**, 287 (2005).
6. G.A. Appignanesi, J.A. Rodríguez Fris, R.A. Montani, W. Kob, Phys. Rev. Lett. **96**, 057801 (2006).
7. E.R. Weeks, J.C. Crocker, A.C. Levitt, A. Schofield, D.A. Weitz, Science **287**, 627 (2000).
8. W.K. Kegel, A. van Blaaderen, Science **287**, 290 (2000).
9. V. Trappe, E. Pitard, L. Ramos, A. Robert, H. Bissig, L. Cipelletti, Phys. Rev. E **76**, 051404 (2007).
10. P. Yunker, Z. Zhang, K.B. Aptowicz, A.G. Yodh, Phys. Rev. Lett. **103**, 115701 (2009).
11. M. Dzugutov, S.I. Simdyankin, F.H. Zetterling, Phys. Rev. Lett. **89**, 195701 (2002).
12. K. Vollmayr-Lee, W. Kob, K. Binder, A. Zippelius, J. Chem. Phys. **116**, 5158 (2002).
13. K. Yoshimoto, T.S. Jain, K. Van Workum, P.F. Nealey, J.J. de Pablo, Phys. Rev. Lett. **93**, 175501 (2004).
14. L. Berthier, R.L. Jack, Phys. Rev. E **76**, 041509 (2007).
15. D. Coslovich, G. Pastore, J. Chem. Phys. **127**, 124504 (2007).
16. C.P. Royall, S.R. Williams, T. Ohtsuka, H. Tanaka, Nat. Mater. **7**, 556 (2008).
17. H. Shiba, A. Onuki, T. Araki, EPL **86**, 66004 (2009).
18. H. Shintani, H. Tanaka, Nat. Phys. **2**, 200 (2006).
19. T. Kawasaki, T. Araki, H. Tanaka, Phys. Rev. Lett. **99**, 215701 (2007).
20. G.S. Matharoo, M.S. Gulam Razul, P.H. Poole, Phys. Rev. E **74**, 050502 (2006).
21. A. Widmer-Cooper, P. Harrowell, H. Fynewever, Phys. Rev. Lett. **93**, 135701 (2004).
22. A. Widmer-Cooper, P. Harrowell, Phys. Rev. Lett. **96**, 185701 (2006).
23. B. Cui, B. Lin, S.A. Rice, J. Chem. Phys. **114**, 9142 (2001).
24. F. Ebert, P. Dillmann, G. Maret, P. Keim, Rev. Sci. Instrum. **80**, 083902 (2009).
25. F. Ebert, P. Keim, G. Maret, Eur. Phys. J. E **26**, 161 (2008).
26. L. Assoud, F. Ebert, P. Keim, R. Messina, G. Maret, H. Löwen, J. Phys.: Condens. Matter **21**, 464114 (2009).
27. L. Assoud, F. Ebert, P. Keim, R. Messina, G. Maret, H. Löwen, Phys. Rev. Lett. **102**, 238301 (2009).
28. F. Ebert, G. Maret, P. Keim, Eur. Phys. J. E **29**, 301 (2009).
29. L. Assoud, R. Messina, H. Löwen, EPL **80**, 48001 (2007).
30. J. Fornleitner, F. Lo Verso, G. Kahl, C. N. Likos, Soft Matter **4**, 480 (2008).
31. S. Mazoyer, F. Ebert, G. Maret, P. Keim, EPL **88**, 66004 (2009).
32. X.H. Zheng *et al.*, Europhys. Lett. **41**, 635 (1998).
33. K. Zahn *et al.*, Phys. Rev. Lett. **85**, 3656 (2000).
34. C. Klix, F. Ebert, G. Maret, P. Keim, arXiv:1108.2636v1.
35. C. Mayer, E. Zaccarelli, E. Stiakakis, C.N. Likos, F. Sciortino, A. Munam, M. Gauthier, N. Hadjichristidis, H. Iatrou, P. Tartaglia, H. Löwen, D. Vlassopoulos, Nat. Mater. **7**, 780 (2008).
36. R. Juárez-Maldonado, M. Medina-Noyola, Phys. Rev. Lett. **101**, 267801 (2008).
37. N. Hoffmann, F. Ebert, C.N. Likos, H. Löwen, G. Maret, Phys. Rev. Lett. **97**, 078301 (2006).
38. N.D. Mermin, Phys. Rev. **176**, 250 (1968).
39. E. Flenner, G. Szamel, Phys. Rev. Lett. **105**, 217801 (2010).
40. H. Tanaka, T. Kawasaki, H. Shintani, K. Watanabe, Nat. Mater. **9**, 324 (2010).
41. U. Schneider, P. Lunkenheimer, A. Pimenov, R. Brand, A. Loidl, Ferroelectics **249**, 89 (2001).
42. We omit the index $_{CR}$ since we always refer to cage-relative quantities in the following.